An Unusual Crystal Growth Method of the Chalcohalide Semiconductor, β-$Hg_3S_2Cl_2$: A New Candidate for Hard Radiation Detection

Arief C. Wibowo.[a] Christos D. Malliakas.[a,b] Hao L,i[a] Constantinos C. Stoumpos,[a] Zhifu Liu,[c] John. A. Peters,[c] Maria Sebastian,[c] Jino Im ,[d] Duck Young Chung,[a] Bruce W. Wessels,[c] Arthur J. Freeman,[d] and Mercouri G. Kanatzidis[a,b]

[a]*Materials Science Division, Argonne National Laboratory, Argonne, Illinois 60439*

[b]*Department of Chemistry*
[c]*Department of Materials Science and Engineering*
and
[d]*Department of Physics and Astronomy,*
Northwestern University, Evanston, Illinois 60208

January 2016

SUBMITTED TO

Crystal Growth and Design

An Unusual Crystal Growth Method of the Chalcohalide Semiconductor, β-$Hg_3S_2Cl_2$: a New Candidate for Hard Radiation Detection

Arief C. Wibowo[a,#], *Christos D. Malliakas*[a,b], *Hao Li*[a], *Constantinos C. Stoumpos*[a], *Zhifu Liu*[c], *John. A. Peters*[c], *Maria Sebastian*[c], *Jino Im*[d], *Duck Young Chung*[a], *Bruce W. Wessels*[c], *Arthur J. Freeman*[d], *Mercouri G. Kanatzidis*[a,b,*]

[a]Materials Science Division, Argonne National Laboratory, Argonne, Illinois 60439; [b]Department of Chemistry, [c]Department of Materials Science and Engineering, and [d]Department of Physics and Astronomy, Northwestern University, Evanston, Illinois 60208.

Keywords: γ-ray Detector, X-ray detector, Semiconductor, Mercury chalcohalide, Crystal growth, Mobility-lifetime product

ABSTRACT

We assess the mercury chalcohalide compound, β-$Hg_3S_2Cl_2$, as a potential semiconductor material for X-ray and γ-ray detection. It has a high density (6.80 g/cm^3), wide band gap (2.56 eV) and crystallizes in the cubic *Pm*-3*n* space group with a three-dimensional structure comprised of [$Hg_{12}S_8$] cubes with Cl atoms located within and between the cubes, featuring a trigonal pyramidal SHg_3 as the main building block. First-principle electronic structure calculations at the density functional theory level predict that the compound has closely lying indirect and direct band gaps. We have successfully grown transparent, single crystals of β-$Hg_3S_2Cl_2$ up to 7 mm diameter and 1 cm long using a new approach by the partial decomposition of the quaternary $Hg_3Bi_2S_2Cl_8$ compound followed by the formation of β-$Hg_3S_2Cl_2$ and an impermeable top layer, all happening in-situ during vertical Bridgman growth. The decomposition process was optimized by varying peak temperatures and temperature gradients using a 2 mm/h translation rate of the Bridgman technique. Formation of the quaternary $Hg_3Bi_2S_2Cl_8$ followed by its partial decomposition into β-$Hg_3S_2Cl_2$ was confirmed by in-situ temperature-dependent synchrotron powder diffraction studies. The single crystal samples obtained had resistivity of 10^{10} Ω·cm and mobility-lifetime products of electron and hole carriers of 1.4(4) x 10^{-4} cm^2/V and 7.5(3) x 10^{-5} cm^2/V, respectively. Further, an appreciable Ag X-ray photoconductivity response was observed showing the potential of β-$Hg_3S_2Cl_2$ as a hard radiation detector material.

Introduction

There is a stronger demand for highly efficient hard radiation (X-rays and γ-rays) detection for the purposes of counter terrorism as well as many scientific and biomedical applications. A material with near-perfect charge transport properties similar to cryogenically-cooled Ge detector[1] and capable of operating at room temperature is the ultimate goal for high resolution hard radiation detectors. This can be achieved with a wide band gap, high mass and density, semiconducting single crystal with extremely low concentrations of electronically active impurities and carrier-trapping defect centers exhibiting high resistivity and high mobility-lifetime products (μτ) for both electrons and holes.

The current leading semiconductors under intensive research for γ-rays detector are $Cd_{1-x}Zn_xTe$ (CZT) and TlBr. In nearly four decades of development, CZT has reached a μτ-product for electrons of ~10^{-2} cm^2/V and an energy resolution of near 2% at 662 keV while TlBr has a μτ-product for electrons of ~10^{-3} cm^2/V and energy resolution of ~2.4%.[2] These high performance compounds, however, come with drawbacks. Low yield along with compositional non uniformity and relatively low μτ-product for holes are the unsolicited features of CZT,[3] and TlBr comes with polarization induced instability at room temperature operation.[4]

We are interested to find a robust, heavy-element containing compound suitable for hard radiation detection. One of the approaches pursued is the so-called "lattice hybridization" in hybrid compound such as chalcohalides.[5] Heavy element-containing chalcohalides are robust hybrid of chalcogenide and halide compounds that possess the desired requirements, i.e., wide band gaps and high density.[5] One particular family of interest are the mercury chalcohalides, $Hg_3Q_2X_2$ (Q = S, Se, Te; X = Cl, Br). These stable compounds possess densities ranging from

6.83 to 7.78 g/cm^3 and band gaps of $2.0 < E_g < 2.6$.[6] Most of these compounds crystallize in high symmetry cubic crystal system and reported, in their respective phase diagram, as congruently melting compounds, favorable for crystal growth.[7]

In previous work, we observed that these compounds and other reported congruently melting semiconductor materials are not "truly" congruent melting during the Bridgman crystal growth process.[5d,6,8] One of our goals is to overcome this problem and establish a novel method and compound that facilitate their growth so that their potential for hard radiation detection can be investigated.

A simple method to grow an incongruent melt compound is by vapor transport, and α- and γ-phase of $Hg_3S_2Cl_2$ crystals, maximum length only up to ~4 mm, were grown using this method, but the β-phase was not reported.[7d] Another method is the use of encapsulating liquid (molten) layer during the crystal growth of Bridgman technique. The inert, low density liquid floats on the top and serves as an encapsulant of the growing compound to maintain its stoichiometry by not letting the volatile part to dissipate. Examples of commonly used encapsulants include B_2O_3 and alkali metal halides.[9] Herein, we report a successful crystal growth of β-$Hg_3S_2Cl_2$ featuring a new hybrid approach involving the formation and partial decomposition of the quaternary $Hg_3Bi_2S_2Cl_8$, a compound reported earlier by us,[5e] which in turn forms an in-situ impermeable top layer that facilitates β-$Hg_3S_2Cl_2$ growth during Bridgman method. This new crystal growth process is discussed and the formation of β-$Hg_3S_2Cl_2$ process was investigated in-situ using a temperature-dependent synchrotron powder diffraction study. The resulting transparent, single crystalline wafers of β-$Hg_3S_2Cl_2$ were characterized in terms of electrical resistivity, mobility-lifetime product, and Ag X-ray detection. The observed optical absorption is correlated with density functional theory band structure calculations.

Experimental Section

Synthesis Chemicals in this work were used without further purification: $HgCl_2$ (99.9995% metal basis, Alfa Aesar), $BiCl_3$ (99.9% metal basis, Alfa Aesar), elemental Hg (99.999%, electronic grade, Sigma-Aldrich), sulfur chunks (99.999%, Spectrum Chemical Mfg. Corp.). All manipulations were done inside a nitrogen-filled glove box. HgS was synthesized as described in our previous publications.[5e,f]

Stoichiometric amounts of $HgCl_2$, HgS, and $BiCl_3$ to synthesize the quaternary $Hg_3S_2Bi_2Cl_8$ with a total mass of 10 grams were ground and loaded into a 9 mm O.D. x 7 mm I.D. x 30 cm long fused silica ampule with a tapered end and subsequently sealed under 10^{-4} mbar vacuum. The reaction mixture was placed in a programmable tube furnace and the temperature was raised to 450 ^{o}C over 12 h, dwelling there for 2 d, followed by cooling to room temperature over 6 h.

Crystal Growth and Sample Preparation The resulting pre-melted ingot filled about one-fourth of the ampule length. Several attempts for crystal growth were performed using combinations of the peak temperatures (360, 450, and 530) and temperature gradients (8, 18, and 28 ^{o}C/cm) set in furnace, all with 2 mm/h translation rates of material through the heating zones. The growth condition which provided the best appearance ingots providing longer (~1 cm long), thus higher yield of transparent β-$Hg_3S_2Cl_2$ with the best transport properties (resistivity, photoconductivity, and Ag Kα X-ray response) from the conditions we attempted was a combination of 450 ^{o}C peak temperature, 18 ^{o}C/cm temperature gradient, and 2 mm/h translation rate.

The single crystal of β-$Hg_3S_2Cl_2$ was obtained from the middle part of ingot with typical dimensions of 1 cm long x 7 mm diameter and was naturally broken-off from the other parts of the ingot. This part was embedded in a wax (Crystal bond 509) inside a rigid plastic pipe and cut

using a precision saw (Struers Secotom 50) and then very carefully machine polished (Buehler Automet 2000) using SiC sandpapers with grits of P280, P1200, P4000 in the order, finished with diamond suspension (0.6 μm) followed by 0.05 μm Al_2O_3 slurry. The final dimensions of each crystal was 4.66 mm long x 3.18 mm wide x 1.57 mm thick in which the resistivity, photoconductivity, and Ag Kα X-ray measurements were conducted.

Powder X-ray Diffraction In order to examine the phase purity of the samples, a small portion was obtained from three different locations along the length of the ingot. The ground powder of three samples taken from the tip (#1), the middle (#2), and the top of the ingot (#3), were used to collect powder X-ray diffraction (PXRD) patterns using a PAnalytical X'Pert Pro Powder Diffractometer (Cu Kα radiation λ = 1.5418 Å) over the 2θ range of 10 - 70^o, with a step size of 0.02^o and a scan speed of 0.25 ^{o}/min.

Laue Back Reflection The Laue back reflection pattern was taken from the fresh, naturally broken-off single crystal sample using The MWL120 Real-Time Back-Reflection Laue Camera from Multiwire Laboratories equipped with Northstar 7 software.

In-Situ Temperature-Dependent Synchrotron Powder Diffraction Study Fine powder of a ground mixture of stoichiometric amounts of $HgCl_2$, HgS, and $BiCl_3$ to synthesize the quaternary $Hg_3S_2Bi_2Cl_8$ was sealed in an N_2-filled Roentgen glass tube. In-situ synchrotron XRD (λ = 0.413906 Å) patterns were recorded from room temperature to 530 ^{o}C and cooling back to room temperature at a rate of 20 ^{o}C/h using the 11-BM beamline at the Advanced Photon Source (Argonne, IL).

UV-Visible Spectroscopy Optical diffuse reflectance measurements were performed at room temperature using a Shimadzu UV-3600 spectrophotometer operating in the 200 – 2500 nm region. The instrument is equipped with an integrating sphere and controlled by a personal

computer. $BaSO_4$ was used as a 100% reflectance standard. The sample (middle part of ingot, #2) was prepared by grinding and spreading it on a compacted surface of the powdered standard material preloaded into a sample holder. The reflectance versus wavelength data generated, were used to estimate the band gap of the material by converting reflectance to absorption data according to Kubelka-Munk equations: $\alpha/S = (1 - R)^2/(2R)$, where R is the reflectance and α and S are the absorption and scattering coefficients, respectively. [10]

Electrical Properties, Photoconductivity Measurements, and Detection Properties Direct current (DC) conductivity was measured with a Keithley Model 617 electrometer using graphite paste (PELCO colloidal graphite, isopropanol base) as conducting material for β-$Hg_3S_2Cl_2$ to establish a good ohmic contact. Photoconductivity was measured using a custom setup as described previously.[5a,8a,11] A diode laser (405 nm) chopped at 589 Hz was focused on the surface of the sample. Graphite electrodes were pasted on the front and back surfaces of the sample in a parallel plate configuration. The μτ-products for electrons and holes were obtained by applying either negative or positive voltage to the illuminated electrode and then measuring the resulting photocurrent for electrons and holes. The output photocurrent signal was collected as the voltage drop on a load resistance R (5 kΩ) and analyzed by the lock-in amplifier. A qualitative measurement of Ag X-ray detection was conducted using a custom setup. A plate crystal sample with dimensions of 4.66 x 3.18 x 1.57 mm^3 was placed inside a guarded box with a copper wire and graphite paste used as the contact. The side of the sample coated with conducting layer was oriented normal to the incoming X-ray beam. The sample was then irradiated by Ag X-ray (22.15 keV, 0.559 Å) with the generator was set at 40 kV and 10 mA. A periodic ON-OFF X-ray state with 3 min each period was applied to the sample for different

applied voltage biases (10, 50, and 100 V). The resulting photocurrent was recorded as a function of time.

The X-ray μτ-product measurement was performed with a low power Ag X-ray source using a AmpTek Mini-X Ag tube operated at 50 kV and 50 μA. Different bias voltages (0, 10, 30, 50, 75, 100, 150, 200, 300, and 500 V) were applied on the same crystal used for the high power X-ray measurement. The X-ray source was switched ON and OFF every 100 s and the photocurrent was recorded continuously as function of time. The X-ray induced photocurrent was calculated by subtracting the X-ray OFF photocurrent from the X-ray ON photocurrent.

Band Structure Calculations We performed the first-principles electronic structure calculations based on the density functional theory formalism using the Projector Augmented Wave method[12] implemented in Vienna Ab-initio Simulation Package.[13] The energy cut off for plane wave basis was set to 350 eV and 6 x 6 x 6 k-point mesh was chosen for Brillouin zone sampling. For exchange-correlation function, the generalized gradient approximation (GGA) was employed within Perdew-Burke-Ernzerhof (PBE) formalism.[14]

Results and Discussion

Synthesis, Crystal Growth, and Sample Preparation β-$Hg_3S_2Cl_2$ crystallizes in a cubic crystal system with *Pm*-3*n* space group (a = 17.925 Å). It has a three dimensional structure with a [$Hg_{12}S_8$] cube with Cl atoms located in the center and between the cubes. The cube was built from a trigonal pyramidal SHg_3 building block with S atoms located in its vertices, Figure 1.[7]

The decomposition of $Hg_3Bi_2S_2Cl_8$ into β-$Hg_3S_2Cl_2$, as reported previously,[5e] inspire us to exploit the decomposition of the quaternary as a new method of growth, in conjunction with

Bridgman technique. Further, the formation of β-$Hg_3S_2Cl_2$ from decomposition of $Hg_3Bi_2S_2Cl_8$ was confirmed using in-situ temperature-dependent powder synchrotron diffraction, Figure 2. As the temperature increases, the starting binaries start to form the quaternary phase at temperature as low as ~220 ^oC, confirming our previous synthetic method, Figures S1, S2.[5e] The partial decomposition of the quaternary into α-$Hg_3S_2Cl_2$, hence a mixture of the quaternary and α-$Hg_3S_2Cl_2$/$BiCl_3$ phases, is observed at ~370 ^oC (Figure S3) which then transitions into β-$Hg_3S_2Cl_2$ at ~390 ^oC. Pure β-$Hg_3S_2Cl_2$ phase persists in the range of ~420 to ~490 ^oC (Figure S4) after which the material starts to melt. During cooling, however, there were no phase match in the observed diffraction patterns to those of the database, hence the phase(s) formed during the crystallization process could not be identified.

Several growth attempts using the $Hg_3Bi_2S_2Cl_8$ formation followed by its partial decomposition into β-$Hg_3S_2Cl_2$ using a three zone vertical furnace were conducted. These attempts involved variations of the following combinations: a) peak temperatures (360, 450, and 530 ^oC), b) temperature gradient (8, 18, and 28 ^oC/cm), all using a translation rate of 2 mm/h. Although there were several conditions that produced good-looking ingots with a transparent area comprising of ¼ length (~1 cm long) of the whole ingot, only one particular condition produced ingots that exhibited the best charge transport properties (resistivity, photoconductivity, and qualitative Ag Kα X-ray response). This was the use of 450 ^oC peak temperature (well within the range of stable β-$Hg_3S_2Cl_2$ phase found in the powder synchrotron diffraction data above), 18 ^oC/cm temperature gradient, and a 2 mm/h translation rate. A representative ingot is shown in Figure 3. The temperature profile used is shown in Figure S5. Henceforth the properties reported below were measured on the crystals grown based on this particular condition.

The phase purity and single crystal quality of the resulting ingot were evaluated using powder X-ray diffraction and Laue back reflection, respectively. The diffraction patterns of three separate specimens that were obtained from different locations along the ingot (#1 was from the tip of the ingot, #2 from the middle, and #3 from the top as shown in Figure 3) were examined. The pattern of the sample #2 obtained from the transparent yellow crystal (~1 cm long constituting about ¼ of the whole length of ingot) matched the simulated pattern of β-$Hg_3S_2Cl_2$ based on the single crystal structure, Figure 4. Further, Laue diffraction confirmed the quality of the single crystal sample, Figure S6. The sample #2 was used for further optical, electrical property, photoconductivity measurements, and assessment of X-ray response.

In PXRD, the sample #1 was composed of β-$Hg_3S_2Cl_2$ as major phase and the quaternary $Hg_3Bi_2S_2Cl_8$ as a minor phase, Figure S7, whereas the sample #3 was predominantly the quaternary $Hg_3Bi_2S_2Cl_8$, Figure S8. A trace mixture of $BiCl_3$, S_2Cl_2, Bi, and $HgCl_2$ was also identified by PXRD in the sample #3, indicating further decomposition had occurred. From these observations, we may infer that the partial decomposition of the quaternary $Hg_3Bi_2S_2Cl_8$ resulted in β-$Hg_3S_2Cl_2$ and other phases, which separated into three different parts along the ingot with compositions as described above, during the vertical Bridgman process. These in-situ separations created a thick impermeable layer (#3), mainly consisting of the quaternary $Hg_3Bi_2S_2Cl_8$, that seems to facilitate single crystal growth of β-$Hg_3S_2Cl_2$ in #2 and prevent its decomposition. This is the first example, to our knowledge, of large crystal growth (~1 cm long and 7 mm diameter) to be demonstrated exploiting the decomposition of more complex phase.

Optical Properties The electronic absorption spectrum obtained from diffuse reflectance spectroscopy at room temperature showed that β-$Hg_3S_2Cl_2$ had a band gap of ~2.56 eV, Figure 5.

Such band gap value is consistent with the yellow colored crystals and in agreement with the previous report.[6,7c]

Electrical Properties, Photoconductivity Measurements, and Detection Properties The room temperature electrical resistivity measured for β-$Hg_3S_2Cl_2$ samples was in the order of 10^{10} Ω·cm. Photoconductivity measurements to obtain μτ-products were conducted on suitably cut and polished single crystal samples using a diode laser. Different voltage polarities were applied to the illuminated sample. The resulting voltage dependence of photocurrent can be modeled as

$$I(V) = \frac{I_0 \mu\tau V}{L^2} \frac{\left(1 - e^{-L^2/\mu\tau V}\right)}{1 + \frac{L}{V}\frac{s}{\mu}} \quad (1)$$

for strongly absorbed light; where I_0 is the saturation current, L is the sample thickness, s is the surface recombination velocity, and V is the applied voltage.[15] The representative photoconductivity curves measured by a diode laser are shown in Figure 6. The estimated μτ-products for electrons and holes are 1.4(4) x 10^{-4} cm^2/V and 7.5(3) x 10^{-5} cm^2/V, respectively. The observed μτ-products are high enough to make β-$Hg_3S_2Cl_2$ a potentially interesting detector material for more detailed investigations aimed at raising the crystal quality and purity of the material. They are comparable to other detector materials, such as CZT,[2a] TlBr,[2c,4] Tl_6SeI_4,[5a] $Cs_2Hg_6S_7$,[16] α-HgI_2,[17] $CsHgInS_3$,[8a] SbSeI,[5d] $CsPbBr_3$,[5c] Tl_6SI_4,[5b] $CsCdInTe_3$,[18] and Tl_4CdI_6[8b] , Table 1.

Upon exposure to Ag X-rays, the β-$Hg_3S_2Cl_2$ sample showed an appreciable response in terms of observed photocurrent as function of time under 10, 50, and 100 V applied biases. Six cycles of the ON-OFF X-ray beam showed consistent behavior without any indication of degradation in all three applied biases, Figure 7. Upon switching off the X-ray beam, the photocurrent decayed slowly and recovery to the dark condition required a few minutes. This long-tail photocurrent decay indicates a slow release of charge carriers from deep trap states, and subsequent

recombination takes place.[19] The absolute photocurrent value increases as the applied bias increases, consistent with the good photoconductivity properties of β-$Hg_3S_2Cl_2$.

High photon intensity sources, like lasers and high power X-rays, usually saturate traps in defective crystals during the excitation measurement resulting in a semi-intrinsic μτ-product, i.e., the apparent μτ-product of the crystal without many defects. Gamma-ray and low power X-ray sources typically produce photons that are comparable in concentration with the number of trapping centers in the crystal. Therefore, measurements with low intensity sources tend to give lower μτ-products due to extensive trapping of most of photo-induced carriers from the high number of traps in a crystal. In any case, when the number of trapping centers in a pure crystal is much lower than the number of absorbed photons and electron-hole pairs created by radiation, the μτ-product values obtained with either high or low intensity sources should be the same for each measurement. We performed photocurrent measurements using low intensity Ag white X-ray (50 kV, 50 μA). X-ray photocurrent signal was still detected under different applied bias and exhibited similar ON-OFF trends with the current obtained using the high intensity X-rays (Figure S9). The resulting X-ray induced photocurrent was plotted against applied bias (Figure 8) giving an estimated μτ-product for electrons to be 3.2(7) x 10^{-5} cm^2/V (obtained by fitting the data by equation (1) for s = 0), smaller than that obtained using laser. The difference of almost one order of magnitude in the μτ-products between the high intensity laser (1.4 x 10^{-4} cm^2/V) and low intensity X-ray (3.2 x 10^{-5} cm^2/V) sources can be attributed to the large number of trapping center in the β-$Hg_3S_2Cl_2$. Nevertheless, the as grown β-$Hg_3S_2Cl_2$ crystal still gives clear and repeatable response to weak Ag white X-rays. Considering that all chemicals used in this β-$Hg_3S_2Cl_2$ crystal growth were utilized without further purification, the observed μτ-products are respectably high. In addition, the fact that β-$Hg_3S_2Cl_2$ exhibits an appreciable X-ray response,

along with its high density, wide band gap, and high crystal symmetry, makes β-$Hg_3S_2Cl_2$ to be one of the potential semiconductor detectors worthwhile for further investigations. Better purification processes combined with further insights in the origin of the formation of phases observed throughout the ingot, may help us in designing and optimizing the condition for β-$Hg_3S_2Cl_2$ crystal formation and growth using our newly found process.

Band Structure To understand the nature of electronic and optical properties of β-$Hg_3S_2Cl_2$, we calculated the electronic band structure and the projected density of states (PDOS). The calculated band structure and PDOS are presented in Figure 9(a) and (b), respectively. In the plots, Fermi level (E_F) is set to zero energy level. The calculated band structure shows that β-$Hg_3S_2Cl_2$ has an indirect band gap. The conduction band minimum (CBM) is located at Γ point and the valence band maximum (VBM) is located at X point. Interestingly, small energy difference (~0.02 eV) of valence band between Γ and X points indicates that the direct transition at Γ point also contributes to the optical transition between band edges, Figure 9(a). This is consistent with the experimental result observed from the sample. Compared to the mostly flat band of VBM, the CBM is isotropic and highly dispersive which supports the experimental observation of the higher μτ value for electrons. The band gap is predicted to be 2.02 eV using the PBE exchange-correlation function. This value is underestimated compared to the experimental band gap of 2.56 eV, which is a well-known tendency of semi-local functions like GGA.

The PDOS calculations suggest that the CBM is composed of Hg-s and S-p orbitals while the VBM is mainly originated from the Cl-p, S-p, Hg-d, and Hg-s orbitals, Figure 9(b). Hg-d orbital is strongly coupled with Hg-s orbital in the energy range from $E-E_F$ = -4 eV to -3 eV. The hybridization between Hg-s and S-p orbitals on the CBM forms the s-like state which is

responsible for the isotropic and highly dispersive characters of the CBM. On the other hand, the lone pairs of Cl-p orbital mainly contribute to the VBM, and also Hg-d orbital and S-p orbital are mixed on the VBM. The lone pairs of Cl-p orbitals lead to the localized character of VBM denoted by the mostly flat band of the VBM.

Conclusions

β-$Hg_3S_2Cl_2$ is a promising compound for high performance X-ray and γ-ray semiconductor detectors under the concept of "lattice hybridization" of wide band gap halides and narrow band gap chalcogenides. First principle electronic structure calculations reveal a highly dispersive CBM, which suggest a high μτ-product for electrons. We have found a new and unusual process to synthesize, grow and stabilize large crystals of β-$Hg_3S_2Cl_2$ using vertical Bridgman technique. The method employs the in-situ processes of formation and decomposition of the quaternary $Hg_3Bi_2S_2Cl_8$ as well as formation of an impermeable top layer that facilitates the growth of β-$Hg_3S_2Cl_2$ single crystal. Further understanding on how such new method works will lead to a higher crystal yield and purity, hence better performance of β-$Hg_3S_2Cl_2$ for hard radiation detection. It may also result in new insights on how to grow other incongruent melting ternary semiconductors. The sample obtained from this process shows high resistivity (~10^{10} Ω·cm) and good μτ-products of ~10^{-4} cm^2/V for both electrons and holes. More importantly, it exhibits a respectable response to Ag X-rays.

Acknowledgment

This work was supported by the Department of Energy, National Nuclear Security Administration, Office of Defense Nuclear Nonproliferation Research and Development and carried out at Argonne National Laboratory under contract No. DE-AC02-06CH11357. Use of

the Center for Nanoscale Materials at Argonne National Laboratory, including resources in the Electron Microscopy Center, was supported by the U.S. Department of Energy, Office of Science, Office of Basic Energy Sciences, under Contract No. DE-AC02-06CH11357. The works in Northwestern University (B.W.W and A.J.F) were supported by a grant from the Department of Homeland Security. This research used resources of the Advanced Photon Source, a U.S. Department of Energy (DOE) Office of Science User Facility operated for the DOE Office of Science by Argonne National Laboratory under Contract No. DE-AC02-06CH11357.

AUTHOR INFORMATION

[#]Current address: Department of Chemistry, Faculty of Science, University of Malaya, Kuala Lumpur, Malaysia, 50603.

Corresponding Author

*To whom correspondence should be addressed. E-mail: m-kanatzidis@northwestern.edu.

Author Contributions

The manuscript was written through contributions of all authors. All authors have given approval to the final version of the manuscript.

Notes

The authors declare no competing financial interest.

REFERENCES

(1) Vetter, K. *Annu. Rev. Nucl. Part. Sci.* **2007**, *57*, 363.
(2) (a) Amman, M.; Lee, J. S.; Luke, P. N.; Chen, H.; Awadalla, S. A.; Redden, R.; Bindley, G. *IEEE Trans. Nucl. Sci.* **2009**, *56*, 795(b) Kim, H.; Churilov, A.; Ciampi, G.; Cirignano, L.; Higgins, W.; Kim, S.; O'Dougherty, P.; Olschner, F.; Shah, K. *Nucl. Inst. and Meth. A* **2011**, *629*, 192(c) Kim, H.; Kargar, A.; Cirignano, L.; Churilov, A.; Ciampi, G.; Higgins, W.; Olschner, F.; Shah, K. *IEEE Trans. Nucl. Sci.* **2012**, *59*, 243.
(3) Bolotnikov, A. E.; Camarda, G. S.; Cui, Y.; Hossain, A.; Yang, G.; Yao, H. W.; James, R. B. *IEEE Trans. Nucl. Sci.* **2009**, *56*, 791.

(4) Hitomi, K.; Matsumoto, M.; Muroi, O.; Shoji, T.; Hiratate, Y. *IEEE Trans. Nucl. Sci.* **2002**, *49*, 2526.

(5) (a) Johnsen, S.; Liu, Z.; Peters, J. A.; Song, J.-H.; Nguyen, S.; Malliakas, C. D.; Jin, H.; Freeman, A. J.; Wessels, B. W.; Kanatzidis, M. G. *J. Am. Chem. Soc.* **2011**, *133*, 10030(b) Nguyen, S.; Malliakas, C. D.; Peters, J. A.; Liu, Z.; Im, J.; Zhao, L. D.; Sebastian, M.; Jin, H.; Li, H.; Johnsen, S.; Wessels, B. W.; Freeman, A. J.; Kanatzidis, M. G. *Chem. Mater.* **2013**, *25*, 2868(c) Stoumpos, C. C.; Malliakas, C. D.; Peters, J. A.; Liu, Z.; Sebastian, M.; Im, J.; Chasapis, T. C.; Wibowo, A. C.; Chung, D. Y.; Freeman, A. J.; Wessels, B. W.; Kanatzidis, M. G. *Cryst. Growth Des.* **2013**, *13*, 2722(d) Wibowo, A. C.; Malliakas, C. D.; Liu, Z.; Peters, J. A.; Sebastian, M.; Chung, D. Y.; Wessels, B. W.; Kanatzidis, M. G. *Inorg. Chem.* **2013**, *52*, 7045(e) Wibowo, A. C.; Malliakas, C. D.; Chung, D. Y.; Im, J.; Freeman, A. J.; Kanatzidis, M. G. *Inorg. Chem.* **2013**, *52*, 2973(f) Wibowo, A. C.; Malliakas, C. D.; Chung, D. Y.; Im, J.; Freeman, A. J.; Kanatzidis, M. G. *Inorg. Chem.* **2013**, *52*, 11875.

(6) Malliakas, C. D.; Wibowo, A. C.; Liu, Z.; Peters, J. A.; Sebastian, M.; Jin, H.; Chung, D. Y.; Freeman, A. J.; Wessels, B. W.; Kanatzidis, M. G. *Proc. SPIE 8507, Hard X-Ray, Gamma-Ray, and Neutron Detector Physics XIV* **2012**, 85070F.

(7) (a) Magarill, S. A.; Pervukhina, N. V.; Borisov, S. V.; Pal'chik, N. A. *Russ. Chem. Rev.* **2007**, *76*, 101(b) Minets, Y. V.; Voroshilov, Y. V.; Pan'ko, V. V. *J. Alloys Compd.* **2004**, *367*, 109(c) Chen, H.-L.; Kuang, H.-M.; Chen, W.-T.; Ying, S.-M.; Liu, J.-H. *J. Chem. Res.* **2009**, 430(d) Carlson, E. H. *J. Cryst. Growth* **1967**, *1*, 271(e) Beck, J.; Hedderich, S. *J. Solid State Chem.* **2000**, *151*, 73(f) Villars, P.; Okamoto, H.; Cenzual, K.; Villars, P., Okamoto, H., Cenzual, K., Eds. www1.asminternational.org, 2013; Vol. 2013.

(8) (a) Li, H.; Malliakas, C. D.; Liu, Z.; Peters, J. A.; Jin, H.; Morris, C. D.; Zhao, L.; Wessels, B. W.; Freeman, A. J.; Kanatzidis, M. G. *Chem. Mater.* **2012**, *24*, 4434(b) Wang, S.; Liu, Z.; Peters, J. A.; Sebastian, M.; Nguyen, S.; Malliakas, C. D.; Stoumpos, C. C.; Im, J.; Freeman, A. J.; Wessels, B. W.; Kanatzidis, M. G. *Cryst. Growth Des.* **2014**, dx.doi.org/10.1021/cg5001446.

(9) (a) Zappettini, A.; Zha, M.; Pavesi, M.; Zanotti, L. *J. Cryst. Growth* **2007**, *307*, 283(b) Zappettini, A.; Marchini, L.; Zha, M.; Benassi, G.; Zambelli, N.; Calestani, D.; Zanotti, L.; Gombia, E.; Mosca, R.; Zanichelli, M.; Pavesi, M.; Auricchio, N.; Caroli, E. *IEEE Trans. Nucl. Sci.* **2011**, *58*, 2352(c) Tallerchik, B. A.; Boiko, S. B.; Shtelmah, S. V. *Semiconductors* **2011**, *45*, 1242(d) Mullin, J. B.; Straughan, B. W.; Brickell, W. S. *J. Phys. Chem. Solids* **1965**, *26*, 782(e) Hoshikawa, K.; Nakanishi, H.; Kohda, H.; Sasaura, M. *J. Cryst. Growth* **1989**, *94*, 643.

(10) (a) Morris, C. D.; Kanatzidis, M. G. *Inorg. Chem.* **2010**, *49*, 9049(b) Kortum, G.; Braun, W.; Herzog, G. *Angew. Chem.* **1963**, *75*, 653(c) Larson, P.; Mahanti, S. D.; Kanatzidis, M. G. *Phys. Rev. B.* **2000**, *61*, 8162(d) McCarthy, T. J.; Tanzer, T. A.; Kanatzidis, M. G. *J. Am. Chem. Soc.* **1995**, *117*, 1294(e) Trikalitis, P. N.; Rangan, K. K.; Bakas, T.; Kanatzidis, M. G. *J. Am. Chem. Soc.* **2002**, *124*, 12255.

(11) (a) Li, H.; Peters, J. A.; Liu, Z.; Sebastian, M.; Malliakas, C. D.; Androulakis, J.; Zhao, L.; Chung, I.; Nguyen, S.; Johnsen, S.; Wessels, B. W.; Kanatzidis, M. G. *Cryst. Growth Des.* **2012**, *12*, 3250(b) Liu, Z.; Peters, J. A.; Wessels, B. W.; Johnsen, S.; Kanatzidis, M. G. *Nucl. Inst. and Meth. A* **2011**, *659*, 333(c) Androulakis, J.; Peter, S. C.; Li, H.; Malliakas, C. D.; Peters, J. A.; Liu, Z.; Wessels, B. W.; Song, J.-H.; Jin, H.; Freeman, A. J.; Kanatzidis, M. G. *Adv. Mater.* **2011**, *23*, 4163(d) Johnsen, S.; Liu, Z.; Peters, J. A.;

Song, J.-H.; Peter, S. C.; Malliakas, C. D.; Cho, N. K.; Jin, H.; Freeman, A. J.; Wessels, B. W.; Kanatzidis, M. G. *Chem. Mater.* **2011**, *23*, 3120.
(12) Blochl, P. E. *Phys. Rev. B.* **1994**, *50*, 17953.
(13) (a) Kresse, G.; Hafner, J. *J. Phys.: Condens. Matter* **1994**, *6*, 8245(b) Kresse, G.; Furthmuller, J. *Phys. Rev. B.* **1996**, *54*, 11169.
(14) Perdew, J. P.; Burke, K.; Ernzerhof, M. *Phys. Rev. Lett.* **1996**, *77*, 3865.
(15) Many, A. *J. Phys. Chem. Solids* **1965**, *26*, 575.
(16) Li, H.; Peters, J. A.; Liu, Z. F.; Sebastian, M.; Malliakas, C. D.; Androulakis, J.; Zhao, L. D.; Chung, I.; Nguyen, S.; Johnsen, S. L.; Wessels, B. W.; Kanatzidis, M. G. *Cryst. Growth Des.* **2012**, *12*, 3250.
(17) (a) Owens, A. J. *J. Synchrotron Radiat.* **2006**, *13*, 143(b) Kargar, A.; Ariesanti, E.; McGregor, D. S. *Nucl. Technol.* **2011**, *175*, 131.
(18) Li, H.; Malliakas, C. D.; Peters, J. A.; Liu, Z.; Im, J.; Jin, H.; Morris, C. D.; Zhao, L. D.; Wessels, B. W.; Freeman, A. J.; Kanatzidis, M. G. *Chem. Mater.* **2013**, *25*, 2089.
(19) Gupta, D.; Brenner, T. J. K.; Albert-Seifried, S.; Lee, M. J.; Heeney, M.; McCulloch, I.; Sirringhaus, H. *Org. Electron.* **2012**, *13*, 36.

Table 1. Mobility-lifetime ($\mu\tau$) products of β-$Hg_3S_2Cl_2$ compared to the current leading semiconductors in γ–ray detector applications.

Compound	$(\mu\tau)_e$ (cm^2/V)	$(\mu\tau)_h$ (cm^2/V)	References
$Cd_{1-x}Zn_xTe$ (CZT)	2.3×10^{-2}	2.4×10^{-5}	1a
TlBr	6.5×10^{-3}	$\sim 10^{-4}$	1c, 3
Tl_6SeI_4	7.0×10^{-3}	6.0×10^{-4}	4a
$Cs_2Hg_6S_7$	1.2×10^{-3}	1.0×10^{-4}	15
α-HgI_2	8.0×10^{-4}	3.0×10^{-5}	16
$CsHgInS_3$	3.6×10^{-5}	2.9×10^{-5}	7a
SbSeI	4.4×10^{-4}	3.5×10^{-4}	4d
$CsPbBr_3$	1.7×10^{-3}	1.3×10^{-3}	4c
Tl_6SI_4	2.1×10^{-3}	2.3×10^{-5}	4b
$CsCdInTe_3$	1.1×10^{-4}	1.3×10^{-5}	17
Tl_4CdI_6	6.1×10^{-4}	1.0×10^{-4}	7b
β-$Hg_3S_2Cl_2$	1.4×10^{-4}	7.5×10^{-5}	This work

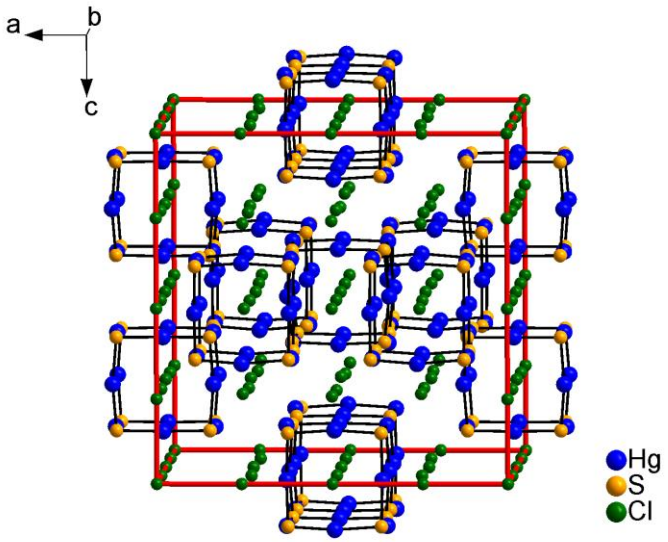

Figure 1. The cubic structure of β-$Hg_3S_2Cl_2$ crystallized in *Pm*-3*n* space group. [7]

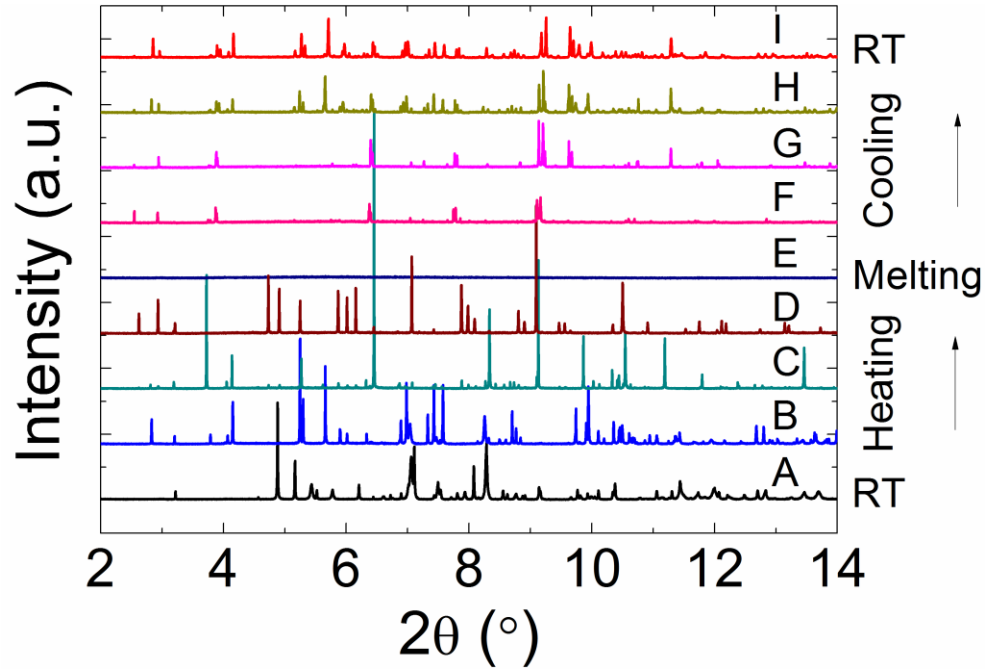

Figure 2. In-situ temperature dependence (heating and cooling) of synchrotron powder XRD patterns (λ = 0.413906 Å) of stoichiometric amounts of $HgCl_2$, 2HgS, and $2BiCl_3$: A) Mixture of the starting binary compounds at room temperature, B) Formation of the quaternary $Hg_3Bi_2S_2Cl_8$ at 220 ^oC, C) Partial decomposition of the quaternary, forming a mixture of both the quaternary and α-$Hg_3S_2Cl_2$ phases, at ~370 ^oC, D) Formation of pure β-$Hg_3S_2Cl_2$ phase at ~420 ^oC, E) Melting of the compound at ~530 ^oC, F) to I) Formation of unidentified phase(s) during cooling.

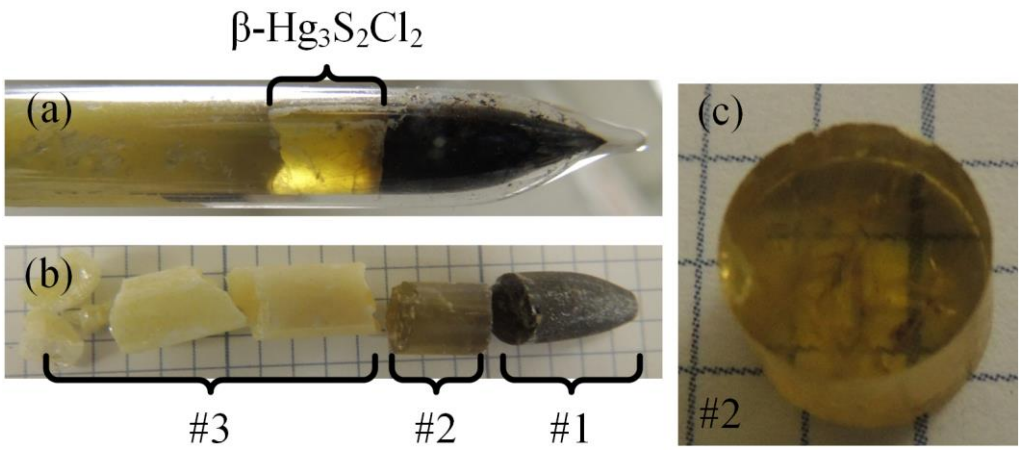

Figure 3. Image of the resulting ingot: (a) before and (b) after taking the ingot out of the tube, showing three separate zones: #1 tip, #2 middle, and #3 top of the ingot, (c) #2 part of the ingot showing a section of pure β-$Hg_3S_2Cl_2$ which was further cut and polished for properties measurements.

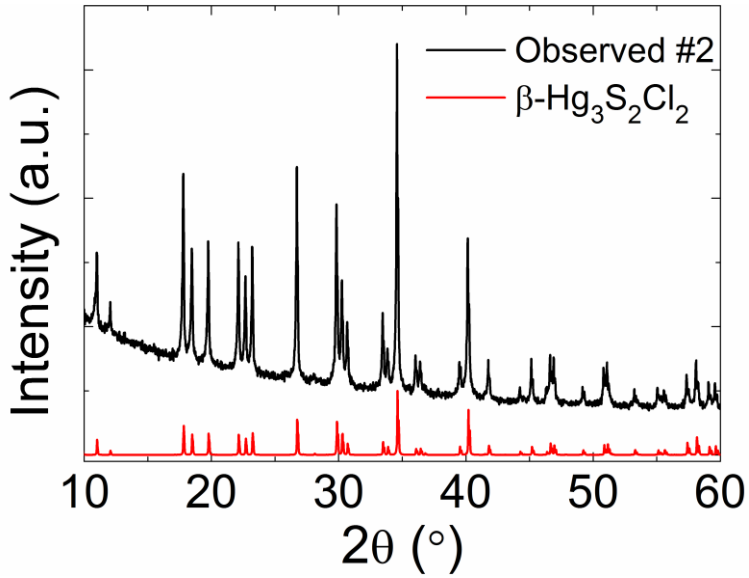

Figure 4. Powder XRD patterns of the resulting ingot part #2 showing a pure β-$Hg_3S_2Cl_2$ phase.

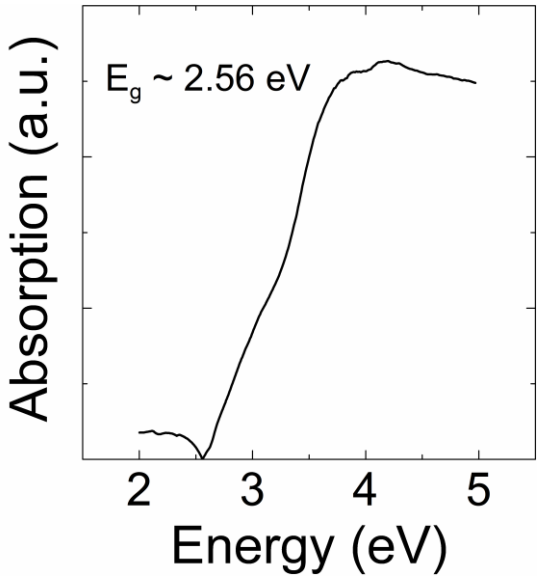

Figure 5. Optical absorption spectrum of β-$Hg_3S_2Cl_2$ with a band gap of ~2.56 eV at room temperature.

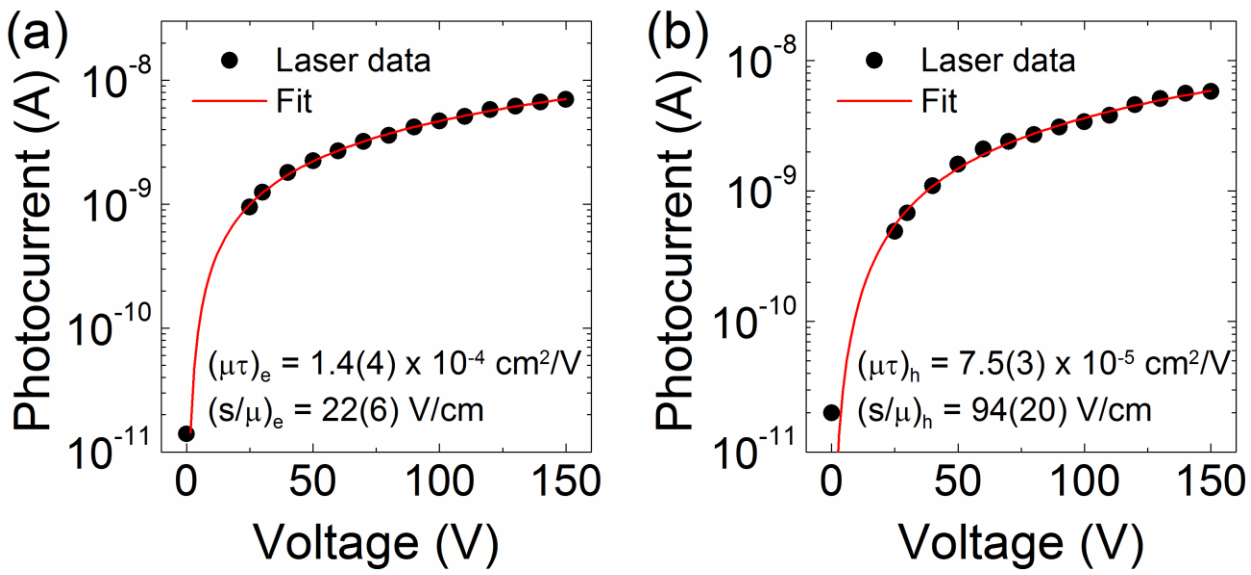

Figure 6. Photocurrent as a function of applied voltage for electrons (a) and holes (b) measured using a diode laser (λ = 405 nm) on a cut and polished β-$Hg_3S_2Cl_2$ single crystal. The $\mu\tau$ products are 1.4(4) x 10^{-4} cm^2/V and 7.5(3) x 10^{-5} cm^2/V for electrons and holes, respectively.

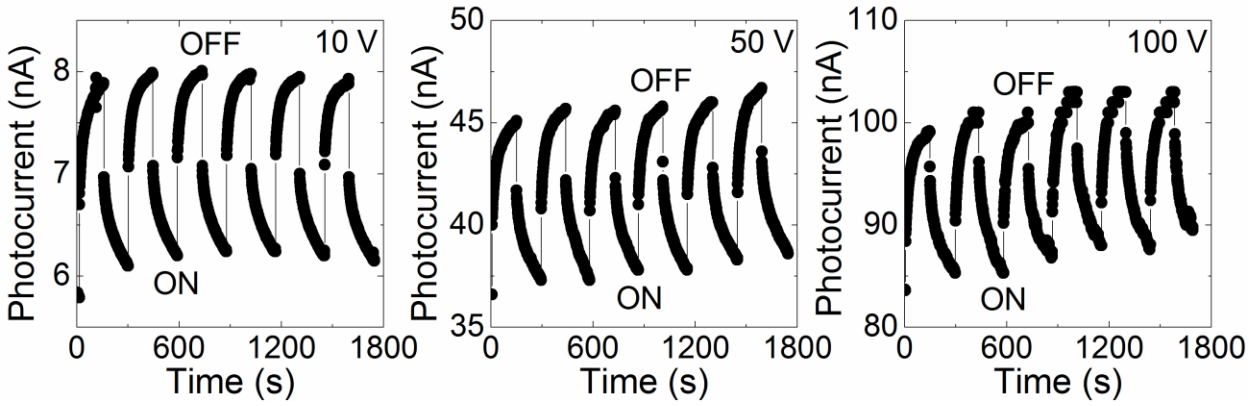

Figure 7. β-$Hg_3S_2Cl_2$ response on Ag Kα radiation with repeated ON and OFF switching of the X-ray beam under different applied biases of 10 V, 50 V, and 100 V.

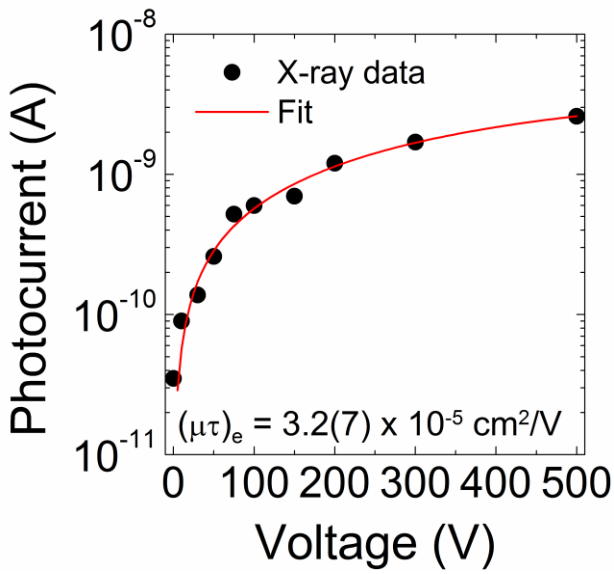

Figure 8. Photocurrent as a function of applied voltage for electrons measured using the Ag white X-ray. The obtained μτ product for electrons is 3.2(7) x 10^{-5} cm^2/V.

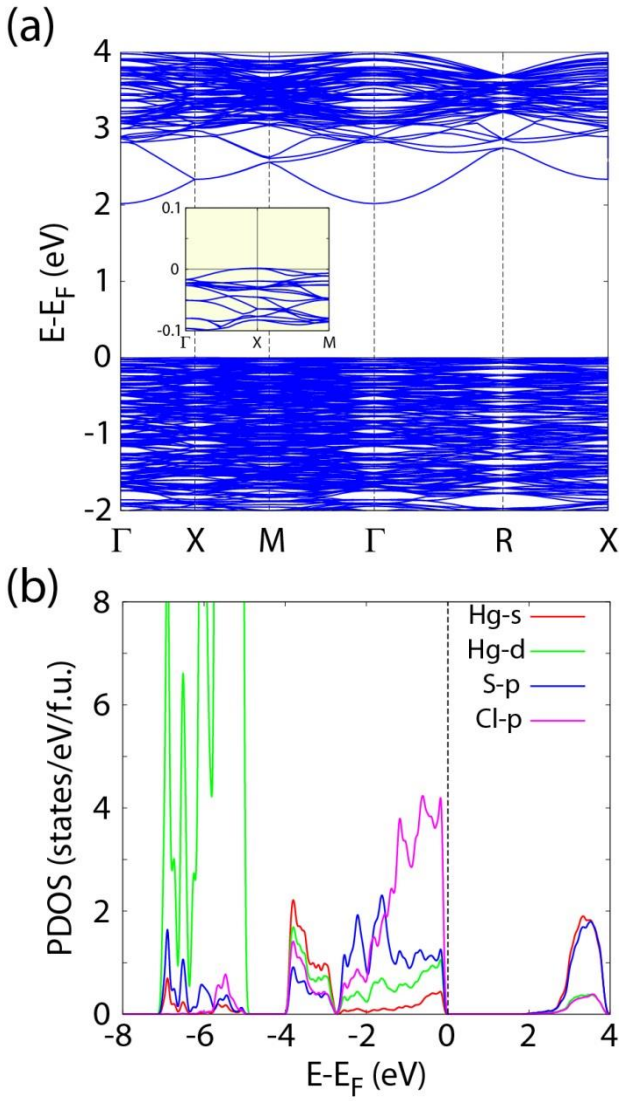

Figure 9. (a) Electronic band structure and (b) projected density of states (PDOS) of β-$Hg_3S_2Cl_2$ are presented. In (a), inset shows a zoomed band structure around X point. In (b), red, green, blue, and violet lines correspond to s-orbital of Hg, d-orbital of Hg, p-orbital of S, and p-orbital of Cl, respectively. In both figures, Fermi levels are set to zero energy level.

TOC

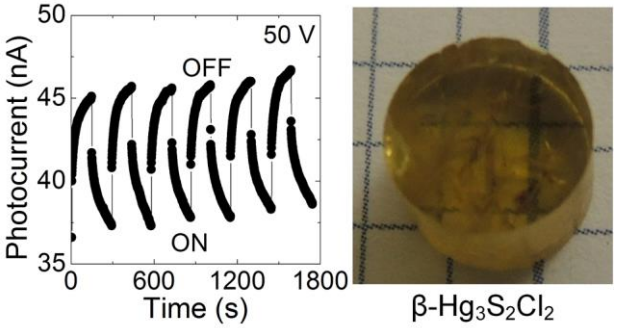
50
45
40
35
Photocurrent (nA)
50 V
OFF
ON
0
600
1200
1800
Time (s)
β-Hg3S2Cl2

An Unusual Crystal Growth of the Chalcohalide Semiconductor, β-$Hg_3S_2Cl_2$: a New Candidate for Hard Radiation Detection

Arief C. Wibowo[a,#], *Christos D. Malliakas*[a,b], *Hao Li,*[a] *Constantinos C. Stoumpos,*[a] *Zhifu Liu*[c], *John. A. Peters*[c], *Maria Sebastian*[c], *Jino Im*[d], *Duck Young Chung*[a], *Bruce W. Wessels*[c], *Arthur J. Freeman*[d], *Mercouri G. Kanatzidis*[a,b,*]

[a]Materials Science Division, Argonne National Laboratory, Argonne, Illinois 60439; [b]Department of Chemistry, [c]Department of Materials Science and Engineering, [d]Department of Physics and Astronomy, Northwestern University, Evanston, Illinois 60208.

SUPPORTING INFORMATION

Table of Contents:

Figure S7. Powder XRD patterns of the resulting ingot part #3 (top of the ingot) showing predominantly the quaternary $Hg_3Bi_2S_2Cl_8$ phase with a trace mixture of $BiCl_3$, S_2Cl_2, Bi, and $HgCl_2$.

Figure S8. Photocurrent induced by Ag white X-ray (50 kV, 50 μA) under different bias voltages.

Figure S9. Photocurrent as a function of applied voltage for electrons measured using the Ag white X-ray. The obtained μτ product for electrons is 3.27×10^{-5} cm^2/V.

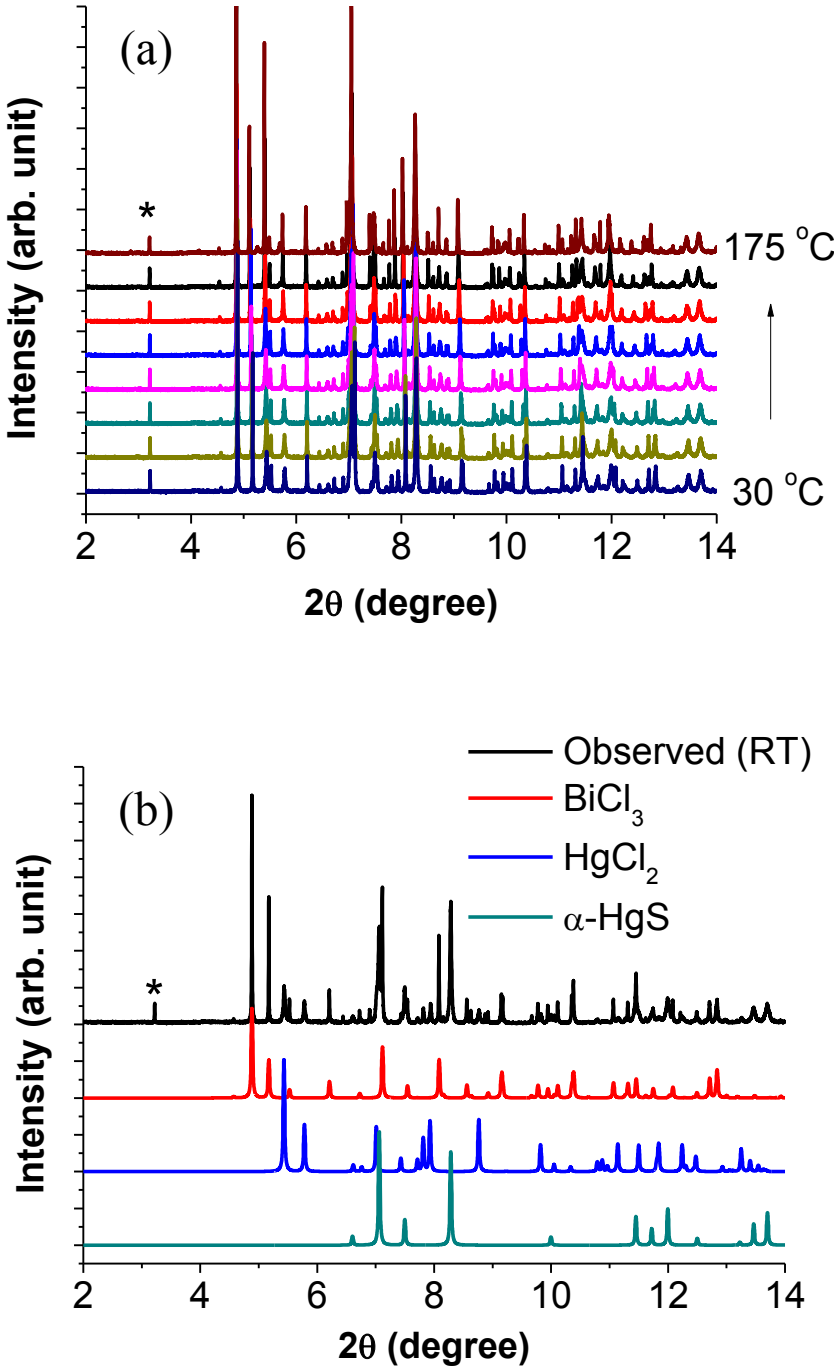

Figure S1. In-situ temperature dependence of synchrotron powder XRD patterns (λ = 0.413906 Å) of stoichiometric amounts of $HgCl_2$, 2HgS, and $2BiCl_3$: (a) on heating from 30 to 175 °C, showing no reaction occurred, (b) The observed pattern at RT (top) showing a mixture of starting binary phases (* = from glass tube).

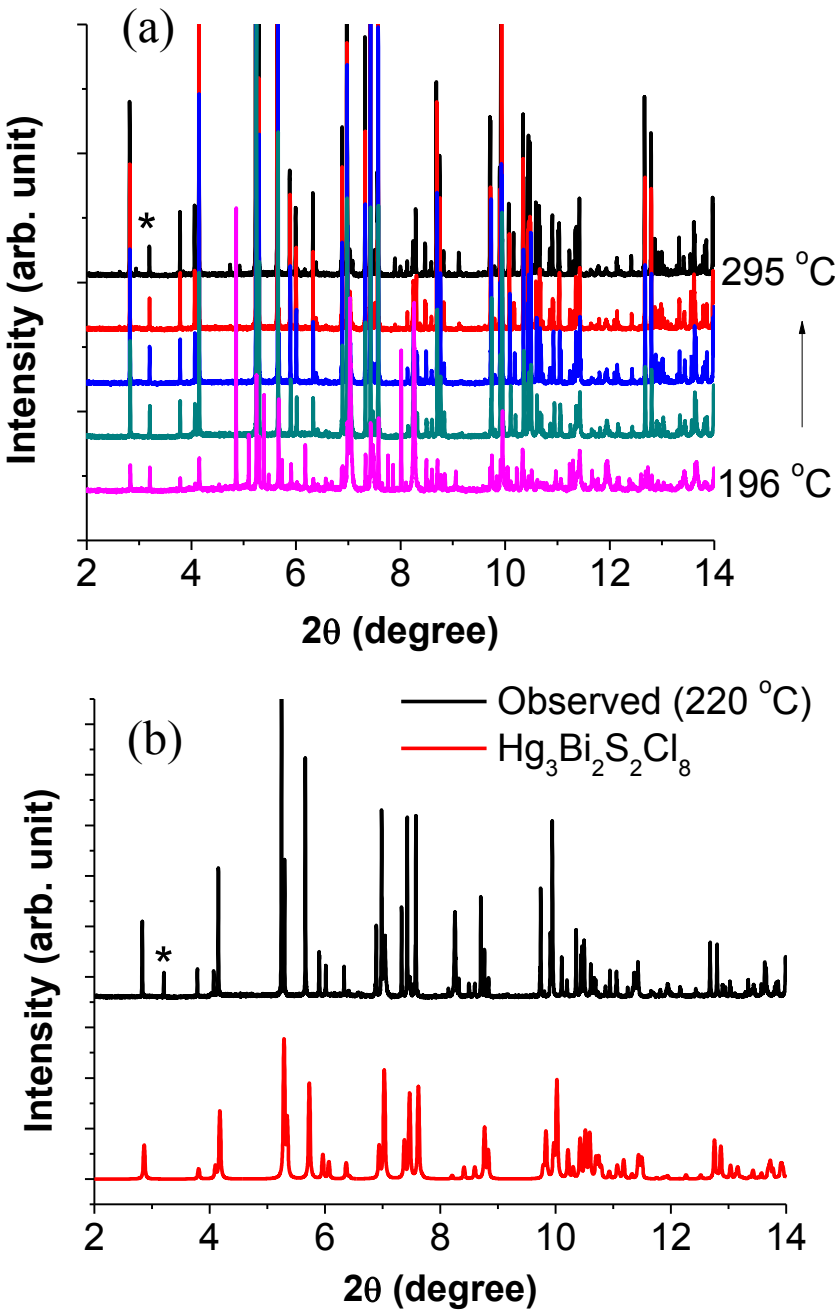

Figure S2. In-situ temperature dependence of synchrotron powder XRD patterns (λ = 0.413906 Å) of stoichiometric amounts of $HgCl_2$, 2HgS, and $2BiCl_3$: (a) on heating from 196 to 295 °C, showing formation of the quaternary $Hg_3Bi_2S_2Cl_8$ phase, (b) The observed pattern at 220 °C (top) showing a pure $Hg_3Bi_2S_2Cl_8$ phase (* = from glass tube).

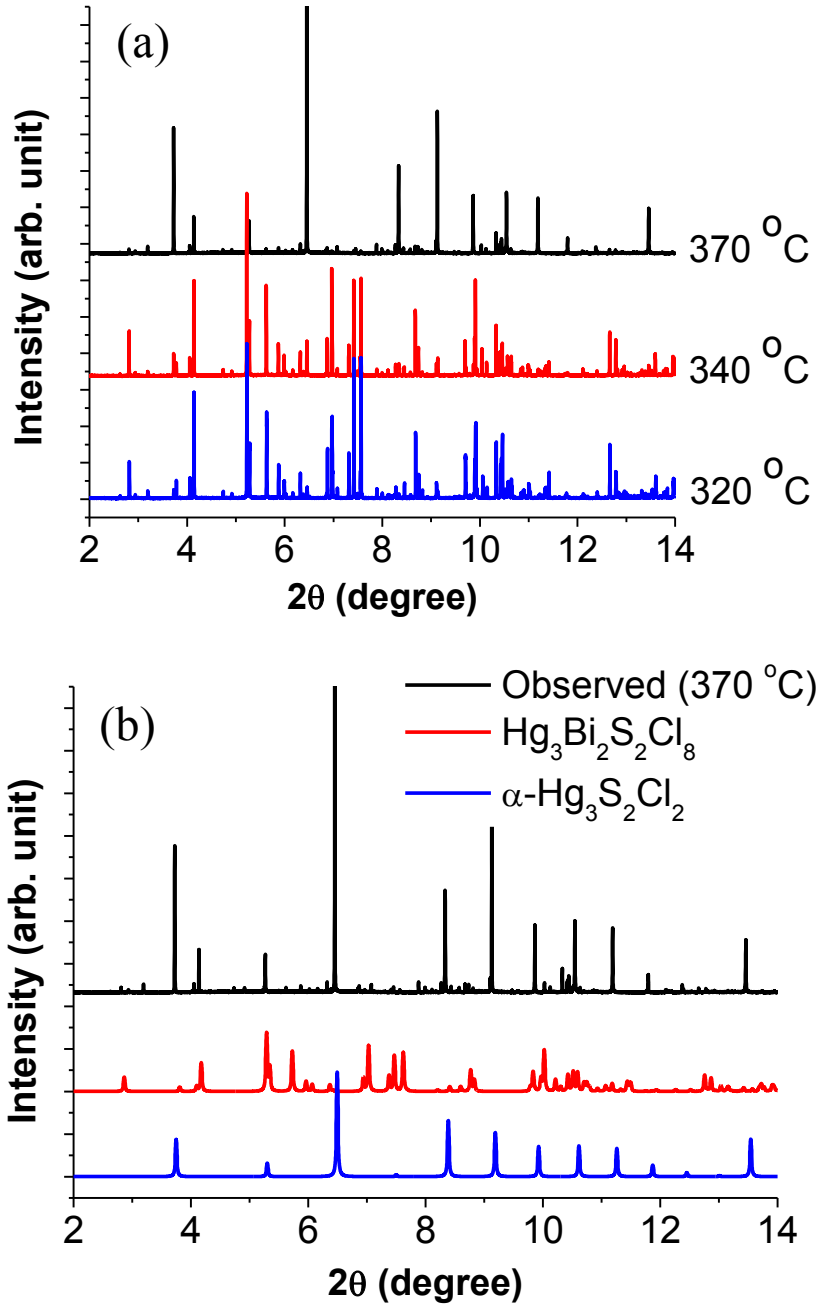

Figure S3. In-situ temperature dependence of synchrotron powder XRD patterns (λ = 0.413906 Å) of stoichiometric amounts of $HgCl_2$, 2HgS, and $2BiCl_3$: (a) on heating from 320 to 370 °C, showing partial decomposition of the quaternary $Hg_3Bi_2S_2Cl_8$ phase into a mixture of itself and α-$Hg_3S_2Cl_2$ phases, (b) The observed pattern at 370 °C (top) showing a mixture of $Hg_3Bi_2S_2Cl_8$ and α-$Hg_3S_2Cl_2$ phases.

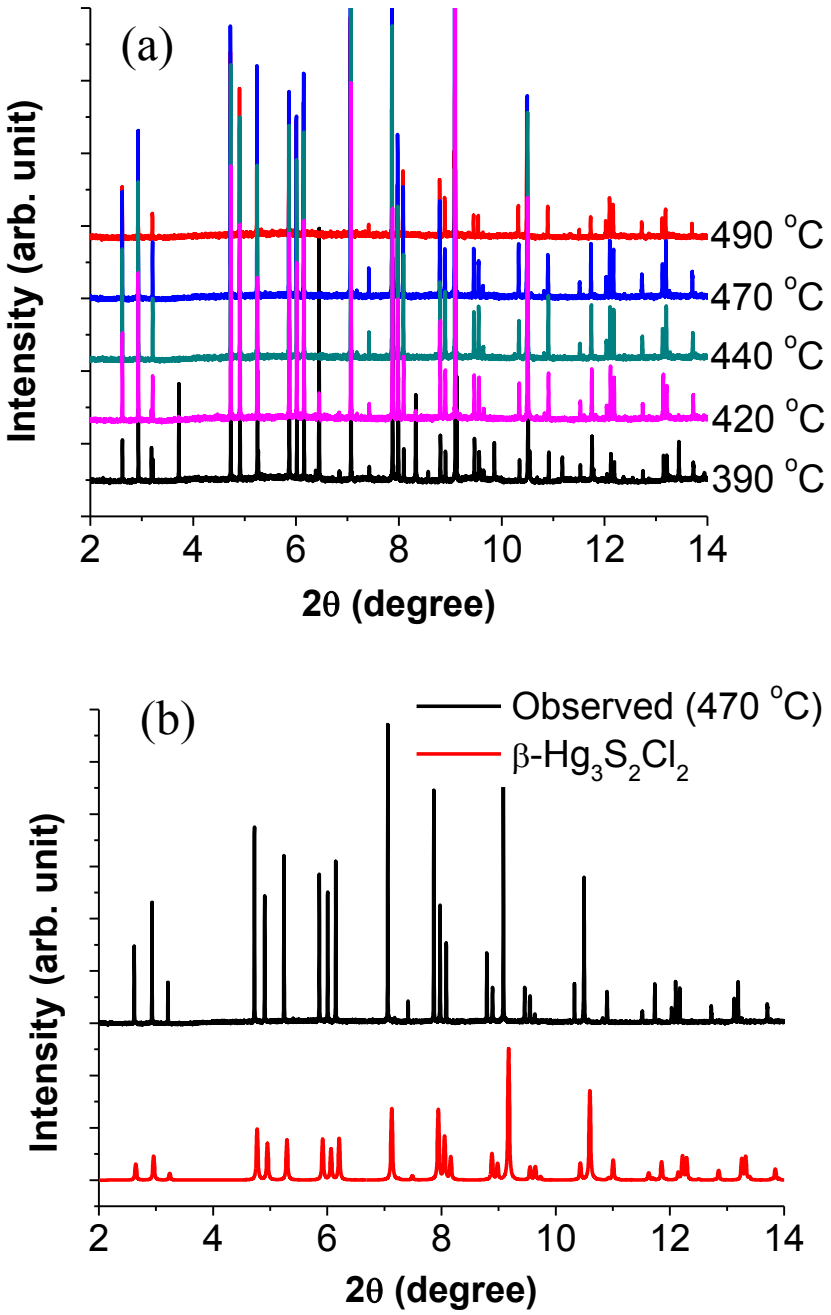

Figure S4. In-situ temperature dependence of synchrotron powder XRD patterns (λ = 0.413906 Å) of stoichiometric amounts of $HgCl_2$, 2HgS, and $2BiCl_3$: (a) on heating from 390 to 490 °C, showing transition into β-$Hg_3S_2Cl_2$ phase at 420 °C, from which the β-$Hg_3S_2Cl_2$ phase is stable up to 490 °C, (b) The observed pattern at 470 °C (top) showing a pure β-$Hg_3S_2Cl_2$ phase.

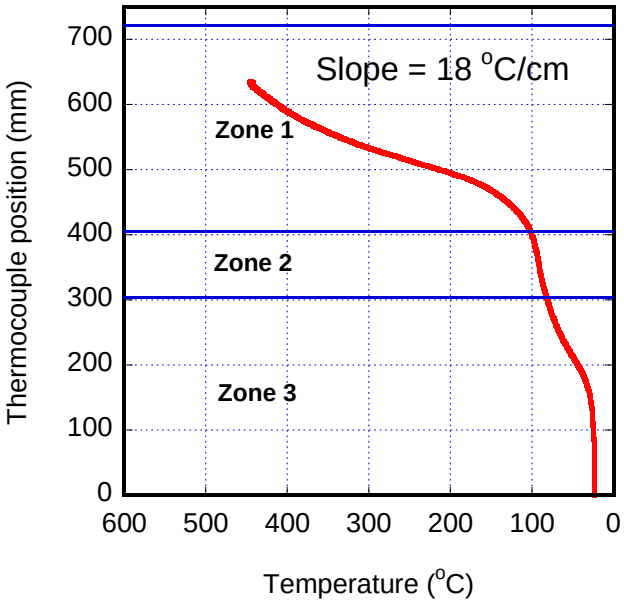

Figure S5. Temperature profile of a three-zone vertical Bridgman furnace used to grow β-$Hg_3S_2Cl_2$ single crystals.

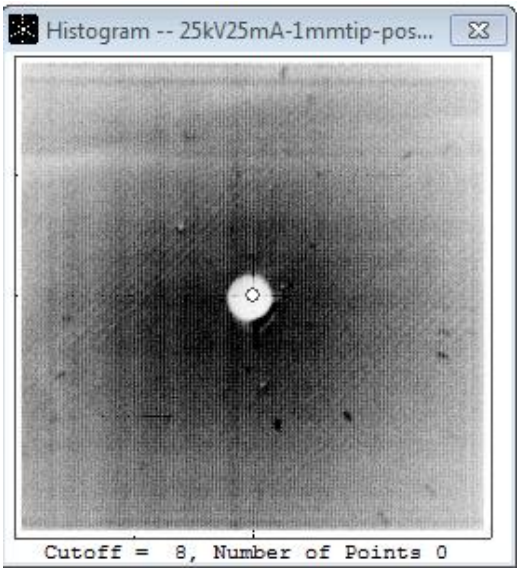

Figure S6. Laue back reflection of β-$Hg_3S_2Cl_2$ wafer recorded using white beam of a W target X-ray tube.

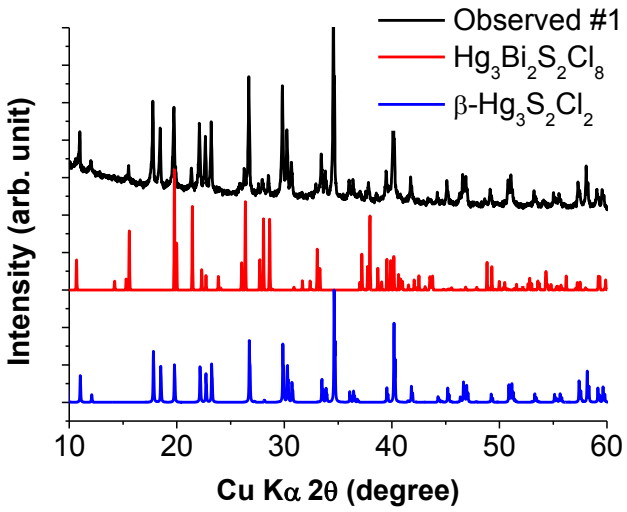

Figure S7. Powder XRD patterns of the resulting ingot part #1 (tip of the ingot) showing a mixture of β-$Hg_3S_2Cl_2$ as major phase and the quaternary $Hg_3Bi_2S_2Cl_8$ as a minor phase.

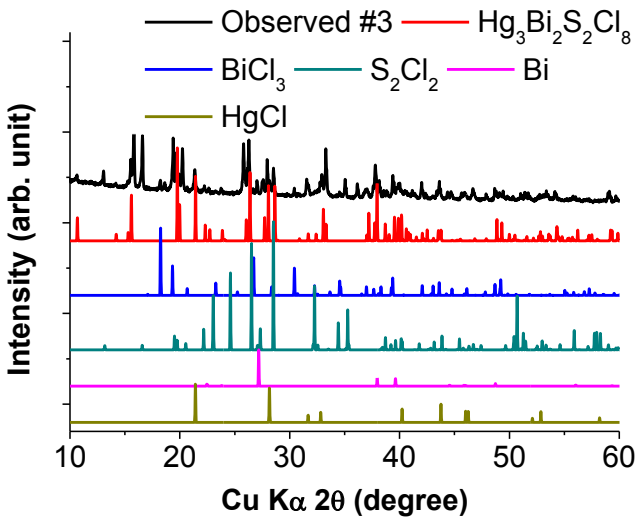

Figure S8. Powder XRD patterns of the resulting ingot part #3 (top of the ingot) showing predominantly the quaternary $Hg_3Bi_2S_2Cl_8$ phase with a trace mixture of $BiCl_3$, S_2Cl_2, Bi, and $HgCl_2$.

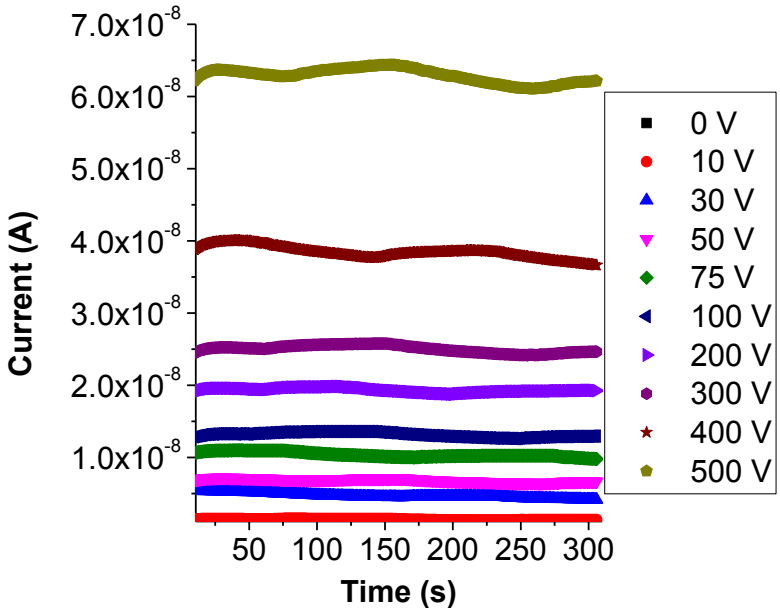

Figure S9. Photocurrent induced by Ag white X-ray (50 kV, 50 μA) under different applied voltages.